Inelastic Deformation and Crosshatching

HARRIS GOLD*
Avco Systems Division, Wilmington, Mass.

AND

RONALD F. PROBSTEIN†
Massachusetts Institute of Technology, Cambridge, Mass.

AND

ROBERT S. SCULLEN‡
Avco Systems Division, Wilmington, Mass.

Probstein and Gold have proposed that crosshatching patterns found on ablated materials are the result of an interaction between an inelastic deformable surface and a supersonic turbulent boundary layer. In this model the patterns can occur in the absence of ablation and are formed as the result of differential deformation due to either relaxation or creep within the material. This paper presents stability calculations which show the effects on the surface pattern characteristics of different boundary-layer profiles and deformation mechanisms. Also presented are detailed surface thickness measurements and pattern statistics on ablated bodies. These data support the proposed model.

Nomenclature

a = speed of sound in boundary layer
$\bar{a}$ = dimensionless speed of sound in boundary layer, a/a_e
c = complex disturbance wave speed
$\bar{c}$ = dimensionless complex wave speed, c/U_e
c_f = skin friction coefficient
$d/d\bar{t}$ = substantial derivative
$D/D\bar{t}$ = linearized substantial derivative, $\partial/\partial\bar{t} + \bar{U}\partial/\partial\bar{x}$
e = shear strain
G = shear modulus
M = $M_e(U - \bar{c})/\bar{a}$
$\bar{M}$ = mean boundary-layer Mach number, $(\bar{U}/\bar{a})\bar{M}_e$
p = pressure
P = $\pi/\bar{\epsilon}$
q = $\sigma/2G$
t = time
$\bar{t}$ = dimensionless time, tU_e/δ
U = boundary-layer velocity profile
$\bar{U}$ = dimensionless boundary-layer velocity profile, U/U_e
v' = normal velocity perturbation
$\hat{v}$ = dimensionless normal velocity perturbation, v'/U_e
x,y,z = Cartesian coordinates, x streamwise, y normal to surface
$\bar{x},\bar{y},\bar{z}$ = dimensionless coordinates, x/δ, y/δ, z/δ
α^* = dimensionless wave number in direction normal to wave front, $2\pi\delta/\lambda$
$\bar{\alpha}$ = dimensionless wave number in x direction, $2\pi\delta/\lambda_x$
$\bar{\beta}$ = dimensionless wave number in z direction, $2\pi\delta/\lambda_z$
γ = specific heat ratio
δ = boundary-layer thickness
ϵ = surface amplitude
$\bar{\epsilon}$ = dimensionless surface amplitude, ϵ/δ
η = surface height
$\bar{\eta}$ = dimensionless surface height, η/δ
θ = wave angle of disturbance
θ^* = phase angle between shear stress and pressure fluctuation
κ = parameter defined by Eq. (14)
κ^* = $\kappa/\cos\theta$
λ = disturbance wavelength in direction normal to wave front
λ_x,λ_z = disturbance wavelengths in x and z directions
μ = viscosity of material
π = disturbance amplitude
$\hat{\pi}$ = pressure perturbation, $(p - p_e)/\gamma p_e$
σ = shear stress
τ = dimensionless material relaxation time, $(\mu/G)(U_e/\delta)$
ϕ = phase angle between pressure and surface
ψ = parameter defined by Eq. (6b)
ω = disturbance frequency
$\bar{\omega}$ = dimensionless disturbance frequency, $\omega\delta/U_e$

Superscripts

$(\ )'$ = fluctuation quantity
$(\ )^*$ = transformed quantities defined by Eq. (4)

Subscripts

e = conditions at edge of boundary layer
I = imaginary part
R = real part
w = conditions at surface

Received July 28, 1970; revision received April 23, 1971. This work was partially supported by the Air Force Space and Missiles Systems Organization under the Advanced Ballistics Re-entry Systems Program, Contract F04-701-69-C-0117.

Index categories: Material Ablation; Boundary Layers and Convective Heat Transfer—Turbulent; Supersonic and Hypersonic Flow.

* Principal Staff Scientist. Member AIAA.

† Consultant, Professor of Mechanical Engineering. Fellow AIAA.

‡ Senior Staff Scientist. Associate Member AIAA.

I. Introduction

CROSSHATCHING refers to the spatially fixed diamond shaped patterns that have been observed to form on the surfaces of ablating bodies. Experimental data indicate that crosshatching only appears when the local boundary-layer edge velocity is supersonic and when the boundary layer is transitional or turbulent.[1] This phenomena has been observed on a wide variety of dissimilar materials including among others, Teflon,[2,3] phenolics,[3] plastics,[1,3-5] camphor,[1,4] and even wood.[3]

Many models have been proposed and analyses carried out to explain the origin and subsequent development of the surface patterns. Most of the analyses involve the model of an interaction of an exterior gaseous boundary layer with a surface gaseous layer resulting from material ablation.[6-11] The boundary-layer flow essentially acts as a phase and amplitude modulator of the small disturbances originating at the interior wavy surface. In the ablation model, under certain super-

sonic conditions the phase and amplitude of the disturbances at the surface are such that resonance occurs in the surface ablation rate and a standing regular crosshatched pattern develops. Still another model and analysis is that of Nachtsheim[12] in which the patterns are considered to form as the result of an interaction between the boundary layer and a surface liquid film. Here the instability results from supersonic wave drag acting on a highly viscous melt layer.

An alternative model to explain the origin of crosshatching which involves neither sublimation nor a liquid melt has been proposed in Ref. 13. Here the surface is considered to be deformable and the crosshatching a consequence of differential deformation due to relaxation and creep within the material. The patterns are not initiated as a result of differential ablation and can form in the absence of ablation. The pattern wavelength imposed on the material by the gaseous boundary layer is of the order of $U\tau$ where U is a characteristic velocity within the boundary layer and τ a characteristic relaxation time for the material. This implies that the pattern geometry is independent of position on the model and that the patterns will form when the material relaxation time becomes comparable with an appropriate characteristic flow time. Figure 1 is a morphological summary of all the analyses thus far carried out.

In Ref. 13 results were presented only for the case of a uniform supersonic Mach number profile and a surface which was modeled as an anelastic Kelvin solid. In this paper nonuniform profiles and other material models are considered. In addition detailed surface measurements are presented for some recovered re-entry vehicles.

II. Analysis

The present analysis is a stability analysis in which the disturbances in the external flow are linearized. The mean external flow is considered to be quasi-parallel and all disturbances three-dimensional and inviscid. The response of the solid is brought in through the introduction of a material stress-strain relation applied at the gas-solid interface. The surface deformation is considered to be linear and periodic. The problem is one in which we seek the conditions under which a material instability develops at the gas-solid interface as a consequence of the response of the deformable surface to the externally modulated pressure fluctuations. The resulting pattern is postulated to be diamond-shaped in the plane of the surface. The instability analysis should then provide the pattern geometry, specifically the wave angle, wavelength, and pattern depth.

External Gaseous Boundary-Layer Flow

The periodic deformable solid surface considered generates disturbances in the gaseous boundary layer which are in turn modulated and reflected back onto the surface. If the amplitude of the surface is sufficiently small then by a straightforward but lengthy analysis the disturbance pressure field $\hat{\pi}$ in the boundary layer can be shown to be described by the following equation (see Ref. 14 for the elements of the derivation)

$$\nabla^2\hat{\pi} - \bar{M}^2\frac{\partial^2\hat{\pi}}{\partial\bar{x}^2} - \frac{d\ln\bar{M}^2}{d\bar{y}}\frac{\partial\hat{\pi}}{\partial\bar{y}} = \frac{\bar{M}_e^2}{\bar{a}^2}\frac{\partial}{\partial\bar{t}}\left[\frac{\partial\hat{\pi}}{\partial\bar{t}} + 2\bar{U}\frac{\partial\hat{\pi}}{\partial\bar{x}} + 2\frac{d\bar{U}}{d\bar{y}}\frac{\hat{v}}{\bar{U}}\right] \quad (1)$$

where the barred dependent variables refer to the mean boundary-layer profiles and $\hat{v}$ is the disturbance velocity normal to the surface. Here it has been assumed that the time dependent perturbation components of each flow quantity are small compared to the mean components and the mean flow is quasi-parallel, i.e., the mean flow is only dependent upon the co-ordinate normal to the surface. It is also assumed that the gas is a calorically perfect one. The slope of the perturbation streamline in the basic flow direction, $\hat{v}/\bar{U}$ is related to the pressure disturbance through the normal momentum equation

$$\frac{D}{D\bar{t}}\frac{\hat{v}}{\bar{U}} = -\frac{\bar{U}}{\bar{M}^2}\frac{\partial\hat{\pi}}{\partial\bar{y}} \quad (2)$$

where $D/D\bar{t} = \partial/\partial\bar{t} + \bar{U}\partial/\partial\bar{x}$ is the linearized substantial derivative.

For parallel and quasi-parallel flows the coefficients of Eqs. (1) and (2) are independent of $\bar{x}$ and $\bar{z}$ and consequently a solution of the form

$$\hat{\pi}(\bar{x},\bar{y},\bar{z},\bar{t}) = \pi(\bar{y})\exp i(\bar{\alpha}\bar{x} + \bar{\beta}\bar{z} - \bar{\omega}\bar{t}), \quad (3)$$

will reduce Eqs. (1) and (2) to ordinary differential equations in $\bar{y}$. The wave numbers $\bar{\alpha}$ and $\bar{\beta}$ are real since the disturbances must be bounded at both $+\infty$ and $-\infty$. The reduced frequency $\bar{\omega}$ is taken to be complex.

The resulting three-dimensional disturbance equations can be reduced to an equivalent two-dimensional form by the following transformations[15,16]

$$\bar{\alpha} = \alpha^*\cos\theta,\ \bar{\beta} = \alpha^*\sin\theta,\ \bar{U} = U^*/\cos\theta$$
$$\bar{\omega}/\bar{\alpha} = \bar{c} = c^*/\cos\theta,\ M = M^*/\cos\theta = \bar{M}_e(\bar{U} - \bar{c})/\bar{a} \quad (4)$$

where θ is the angle between the wave normal and the x axis. The crosshatch pattern angle is the complement of this angle.

Introducing Eqs. (3) and (4) into Eqs. (1) and (2) we obtain the following equation for the pressure disturbance amplitude $\pi(\bar{y})$:

$$d^2\pi/d\bar{y}^2 - (d\ln M^{*2}/d\bar{y})d\pi/d\bar{y} + \alpha^{*2}[M^{*2} - 1]\pi = 0 \quad (5)$$

Here the disturbance amplitude π and M^* are complex.

The boundary condition on π for large values of $\bar{y}$ is determined from Eq. (5) itself. As $\bar{y}\to\infty$, $\bar{U}\to 1$, and $\bar{a}\to 1$ with the result that Eq. (5) takes the limiting form

$$d^2\pi/d\bar{y}^2 + \alpha^{*2}\psi^2\pi = 0 \quad (6a)$$

where

$$\psi^2 = M_e^{*2} - 1 = \bar{M}_e^2[1 - \bar{c}_R - i\bar{c}_I]^2\cos^2\theta - 1 \quad (6b)$$

Here $\bar{c}_R$ and $\bar{c}_I$ are the real and imaginary parts of the complex wave speed $\bar{c}$ defined by Eq. (4). By imposing the condition that all waves at infinity must be bounded and outgoing the boundary condition at infinity can be written as

$$d\pi/d\bar{y} + i\alpha^*\psi\pi = 0 \quad (7)$$

where $-180° < \arg\psi^2 < 180°$.

The disturbances are classified as subsonic (Real $\psi^2 < 0$), sonic (Real $\psi^2 = 0$), and supersonic (Real $\psi^2 > 0$) according to whether the phase velocity of the disturbance relative to the freestream velocity and in the direction of the normal to the wave front is less than, equal to, or greater than the mean speed of sound in the freestream. For example, for $\bar{c}_I = 0$ these conditions can be written as $1 - (\bar{M}_e\cos\theta)^{-1} < c_R < 1$ (subsonic), $\bar{c}_R = 1 - (\bar{M}_e\cos\theta)^{-1}$ (sonic) and $\bar{c}_R < 1 - (\bar{M}_e$

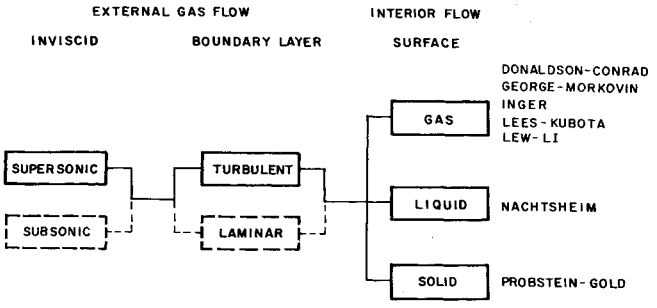

Fig. 1 Crosshatching analyses morphology.

$\cos\theta)^{-1}$ (supersonic), where $\bar{M}_e \cos\theta$ is the local boundary-layer edge Mach number normal to the wave front.

The flow is unstable, neutrally stable, or stable to the disturbance waves according to whether the imaginary part of the wave speed c_I is positive, zero, or negative, respectively. The temporal amplification rate of the disturbance is defined as $\alpha^* c_I^* = \bar{\alpha}\bar{c}_I$.

The boundary condition at the solid surface is determined by the condition that there must be zero normal relative velocity between the fluid and the wall, i.e.,

$$\hat{v} = D\bar{\eta}/D\bar{t} \tag{8}$$

where $\bar{\eta} = \bar{\epsilon} \exp i\alpha^*(x^* - c^*\bar{t})$ designates the dimensionless surface height. The pressure gradient at the wall is related to the surface displacement through Eqs. (2) and (8) to give at the surface

$$d\pi/d\bar{y} = \bar{\epsilon}\alpha^{*2}M^{*2} \tag{9}$$

Equation (5) together with the boundary conditions Eqs. (7) and (9) define the pressure perturbation. Since these equations are homogeneous we can eliminate the parameter $\bar{\epsilon}$ by introducing a new variable $P = \pi/\bar{\epsilon}$. In this case the solution of these equations is defined once the wave number α^* and the Mach number profile $M^*(\bar{y})$ relative to the wave speed $\bar{c}$ are given.

The validity of the assumptions leading to Eq. (9) must be examined. First, the amplitude of the surface $\bar{\epsilon}$ must be small compared with the wavelength of the disturbance, $\lambda = 2\pi\delta/\alpha^*$, so that $(\bar{\epsilon}\alpha^*)^2$ is negligibly small. It might appear that an additional restriction must be placed on $\bar{\epsilon}$ if the mean velocity gradient near the wall is large, e.g., for turbulent flows. The restriction would be that $\bar{\epsilon}$ be small in comparison with the height over which the velocity changes appreciably, e.g., the depth of the turbulent sublayer. By using an orthogonal curvilinear coordinate system in which the surface is a coordinate line and where the mean velocity profile bends to follow the surface wave, Benjamin[17] showed that such an additional restriction on $\bar{\epsilon}$ is not necessary.

In this analysis we have assumed that the pressure perturbation field can be calculated from inviscid stability theory. Benjamin[17] showed that the phase shift and amplitude due to the effect of finite viscosity on the pressure fluctuations can be neglected. For neutral disturbances and $c_R^* = 0$ the surface $\bar{y} = 0$ is a nonessential singular point of Eq. (5) since $\bar{U} = 0$. However, the pressure disturbance is generated by the inviscid behavior of the mean flow and is essentially constant across the layer near the wall where the viscous and inviscid forces balance each other. Therefore, the pressure perturbation at the wall can be obtained by evaluating Eqs. (5) and (9) at a small distance $\bar{y} = \bar{y}_0$ away from the surface.

Boundary Layer—Deformable Surface Interaction

The boundary condition at the surface introduces the material response since at the wall $\bar{y} = \bar{\eta}$ the slope of the perturbation streamline must be continuous [see Eq. (2)] and its value is determined by the local surface deformation [Eq. (8)]. We shall consider two limiting deformable surface models[18]: a Kelvin body and a Maxwell body, recognizing, however, that depending upon the material being considered, other relaxation and creep relations governing the material response might be more appropriate.

The defining equations for the shear strain e are[18]

Kelvin $$\tau de/d\bar{t} = q - e \tag{10a}$$

Maxwell $$\tau de/d\bar{t} = \tau dq/d\bar{t} + q \tag{10b}$$

where $q = \sigma/2G$, with σ the shear stress in the body, G the shear modulus, $\tau = (\mu/G)(U_e/\delta)$ the dimensionless material relaxation time, and μ the viscosity of the material. The shear strain fluctuation can be obtained in terms of the shear stress fluctuation by linearizing the preceding equations:

Kelvin $$\tau De'/D\bar{t} = q' - e' \tag{11a}$$

Maxwell $$\tau De'/D\bar{t} = \tau Dq'/D\bar{t} + q' \tag{11b}$$

The local surface deformation is related to the local strain fluctuation by $e' = \partial\eta/\partial x$ (for $\lambda \gg \eta$) and the shear stress fluctuation σ' to the pressure perturbation by

$$q' = \sigma'/2G = \kappa\hat{\pi}e^{i\theta^*} \tag{12}$$

Here κ is a parameter measuring the proportionality between the fluctuations in surface pressure and shear stress, and θ^* is the phase angle between the stress and pressure fluctuations.

By taking the real and imaginary parts of Eqs. (11) we obtain

Kelvin $$\alpha^*\tau\cdot\alpha^* c_I^* = \alpha^*[-1 + (\kappa^*/\alpha^*)P_w \sin(\phi + \theta^*)] \tag{13a}$$

Maxwell $$= \kappa^* P_w \sin(\phi + \theta^*) \tag{13b}$$

Kelvin, Maxwell $$\alpha^*\tau c_R^* = (\kappa^*/\alpha^*)P_w \cos(\phi + \theta^*) \tag{13c}$$

Here P_w is the amplitude of the pressure disturbance at the wall, ϕ is the angle between the surface pressure fluctuation and the surface, and $\kappa^* = \kappa/\cos\theta$. In deriving Eqs. (13b) and (13c) for the Maxwell body it has been assumed that $\kappa^* P_w/\alpha^* \ll 1$, thereby simplifying the form of the equations. This approximation is justified since as shown below $\kappa <<< 1$ and $P_w/\alpha^* \sim 0(1)$.

From Eq. (12) and by identifying the gaseous shear stress at the wall with σ, it follows that

$$\kappa \sim (p_e M_e^2/2G)c_f \tag{14}$$

where c_f is the skin-friction coefficient for the boundary-layer flow. Some typical values of these constants are G $\sim$ 300–600 atm for Teflon and $c_f \sim 10^{-4}$ for turbulent flow. If $p_e \sim 1$ atm and $M_e \sim 10$ then $\kappa \sim 0(10^{-4})$; the numerical calculations to be discussed below show that $P_w/\alpha^* \sim 0(1)$. Therefore we conclude that the disturbance flow is stable for the Kelvin body [see Eq. (13a) with $\kappa^* P_w/\alpha^* \ll 1$] and unstable for the Maxwell body [see Eq. (13b)] when $\phi + \theta^*$ lies in either the first or second quadrants.

In Ref. 13 an instability was indicated for a Kelvin body in constrast to the present results. This stems from the fact that there only a uniform inviscid profile was considered, for which there is no phase lag between the pressure and shear stress fluctuations. Furthermore, for the uniform profile the surface pressure fluctuations are large, $\kappa^* P_w/\alpha^* > 1$ and the right hand side of Eq. (13a) is positive leading to instability. The simplified model of Ref. 13 is therefore indicative of the inelastic deformation type of instability and is correct for the limit discussed there.

Results

The results of the stability calculations for both the external gaseous boundary-layer flow and the deformable surface will now be presented. As already noted the amplitude and phase of the surface pressure perturbations do not depend upon the surface deformation model. They can be determined as a function of the wave number and wave angle by solving Eq. (5) subject to the boundary conditions Eqs. (7) and (9). These equations have been solved previously by Lees and Kubota,[10] also in connection with the crosshatching problem, for a turbulent Mach number profile. These calculations are here extended to include laminar and stepped profiles.

The stability characteristics of the deformable surface depend on the particular surface deformation model and the amplitude and phase angle characteristics of the surface pressure perturbation. The wave speed and amplification rate

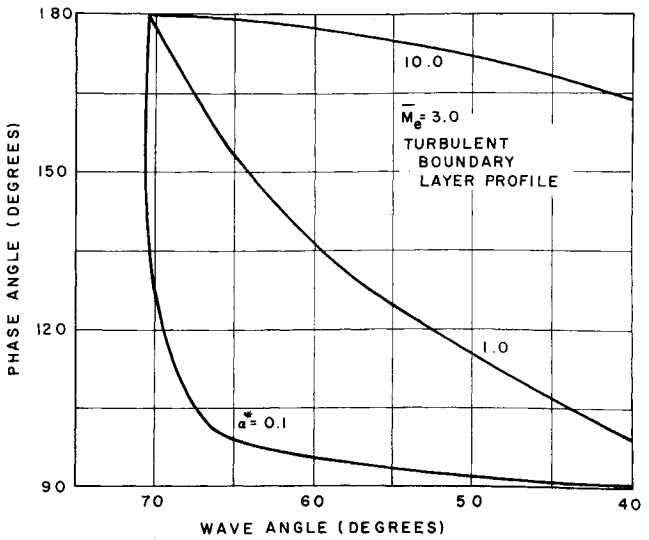

Fig. 2 Phase angle-wave angle relationship for a turbulent boundary-layer Mach number profile.

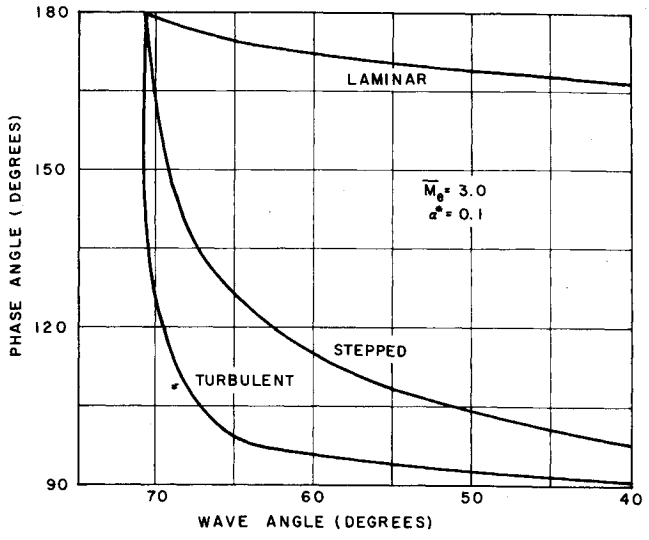

Fig. 3 Phase angle-wave angle relationship for different boundary-layer Mach number profiles.

are determined from Eqs. (13) as a function of both the wave angle and wave number. These results are given below for the Maxwell body following the presentation of the results for the surface pressure perturbations.

Surface Pressure Perturbations

By introducing the transformation, $H = (dP/d\bar{y})/\alpha^{*2}M^{*2}P$, Eq. (5) can be reduced to a first-order nonlinear Ricatti equation for H in which the Mach number gradient term has been eliminated. The numerical integration of this equation was carried out on an IBM 360 using a standard Runge-Kutta numerical technique. The integration was made for a given value of the wave number. It was started from the point where the Mach number profile is sensibly uniform (the edge of the boundary layer) and proceeded inward towards the wall. The integration was carried to a small distance $\bar{y} = \bar{y}_0$ away from the mean position of the wall. For our calculations $\bar{y}_0$ was taken to be equal to 0.003. It should be noted that at $\bar{y}_0$ the pressure disturbance $P(\bar{y} = \bar{y}_0) \approx H^{-1}(\bar{y} = \bar{y}_0)$.

Both the time rate of amplification ($\bar{c}_I$) and the wave speed ($\bar{c}_R$) were taken to be zero. Sample calculations were carried out for $\bar{c}_R = 0$ and for values of $\bar{c}_I$ as large as 0.5. They showed that only the quantitative nature of the pressure amplitude and phase were changed and then only by a small amount. Although calculations were not done for values of $\bar{c}_R$ other than zero, it may be expected that the same conclusion would apply. We would point out that the wave speed $\bar{c}_R$ is characterized by some laminar sublayer speed, which is at most equal to 0.5.

Figure 2 shows the phase angle relationship between the pressure and the surface for a typical turbulent boundary-layer Mach number profile with an edge Mach number of 3.0 and a wall to edge temperature ratio of unity. It is clear that for the low wave numbers the boundary layer behaves as if it were uniform and supersonic, while for high wave numbers only the subsonic portion of the boundary layer near the wall is important even though the outer portion of the boundary layer is supersonic. These results are also typical for higher boundary-layer edge Mach numbers.

Figure 3 shows the effect of different boundary-layer Mach number profiles on the surface pressure phase angle for a low wave number. The laminar velocity profile was taken to be a Blasius one, while the stepped profile is almost uniform at 0.4 of the freestream velocity up to one-half the boundary-layer thickness; over the remaining portion of the boundary layer the velocity is close to the freestream velocity. The Crocco integral with a value of the wall to freestream temperature of unity was used to obtain the Mach number profiles. The laminar profile acts as if it were subsonic, even for the low wave number shown, while the stepped profile behaves as if it were mainly supersonic. At the higher wave numbers all the profiles behave subsonically (cf. Fig. 2).

Deformable Surface Characteristics

The stability characteristics of the Maxwell body are given by Eqs. (13) in terms of the wave number of the disturbance α^*, the amplitude P_w and phase angle ϕ of the surface pressure, and the phase angle between the surface pressure and shear stress fluctuations θ^*. Since, as pointed out previously, P_w and ϕ are weak functions of c_I^* and c_R^*, the amplification rate and wave speed can be determined to first order by using the calculations of the surface pressure fluctuations for $c_I^* = c_R^* = 0$.

The phase angle θ^* is determined by employing a result of Benjamin.[17] Specifically, Benjamin has shown that for incompressible flow over a wavy surface the shear stress lags the pressure at the surface by 120°. Further Lees and Reshotko[19] show that in the vicinity of the critical point the effect of compressibility can be neglected. It therefore appears that Benjamin's result is also applicable for compressible flows. It should be pointed out this result is only valid when the critical point, i.e., the position in the boundary layer at which the flow velocity is equal to the wave velocity, lies near to or at the surface. This is a limitation of the results to be presented. In the numerical calculations that follow θ^* will be taken to be equal to $-120°$ [the minus sign follows from Eq. (12)]. Since $\phi + \theta^*$ must lie in the first and second quadrants for amplified disturbances, $120° \leqslant \phi \leqslant 300°$. However, the results of the surface pressure calculations show that the phase of the surface pressure lies between $90° < \phi <$

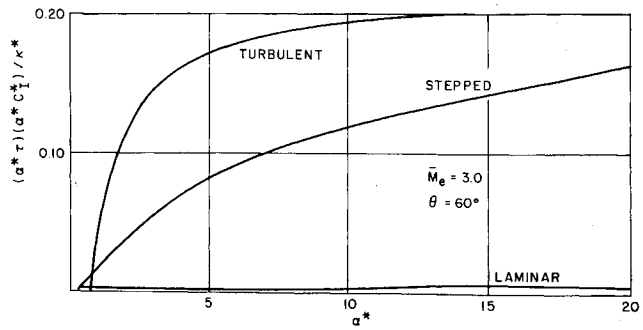

Fig. 4 Amplification rate for different boundary-layer Mach number profiles.

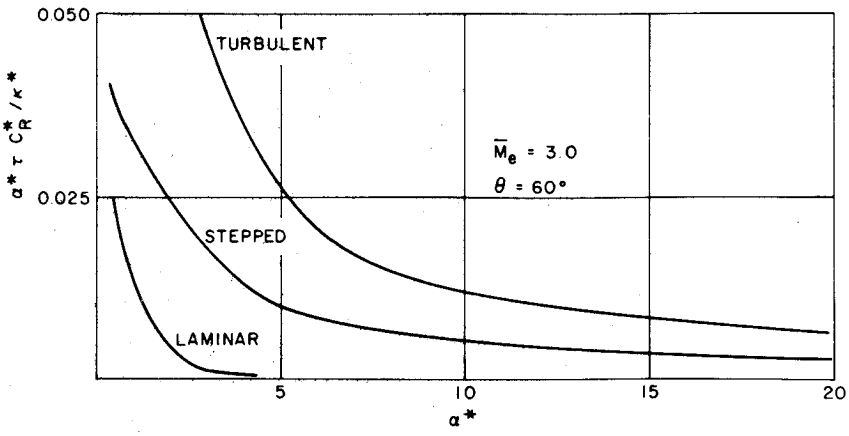

Fig. 5 Disturbance wave speed for different boundary-layer Mach number profiles.

180°. We shall therefore seek those combinations of wave number and sweep angle for which $120° \leqslant \phi \leqslant 180°$. For these cases $c_R^* > 0$.

The surface phase angle characteristics for the three different Mach number profiles show that an instability develops for all three profiles. The strength of the instability depends upon the amplification rate of the responding surface. Figure 4 is a plot of $\alpha^*\tau \cdot \alpha^* c_I^*/\kappa^*$ [see Eq. (13b)] as a function of the wave number α^* for the three profiles considered. The ordinate is a measure of the amplification rate. The amplification rates for both the turbulent and stepped profiles are two orders of magnitude larger than those for laminar flow, with the turbulent rate the highest. These results show that the laminar profile is least capable of producing a resonant condition.

Up to this point we have only considered cases for which the edge Mach number normal to the wave is supersonic. When the normal edge Mach number is subsonic, the surface phase angle for the pressure disturbances is always 180° and the flow is unstable for a Maxwell body. However, the amplification rates are lower than those for supersonic flow so that all other conditions being equal we may expect to obtain the resonant condition for the supersonic case.

In inviscid instability analyses the most unstable disturbance wavelength or frequency is generally determined from the condition of a maximum in the amplification rate (see, e.g., Ref. 20). Figure 4 shows that for a given wave angle $\alpha^*\tau \cdot \alpha^* c_I^*/\kappa^*$ does not have a maximum as a function of wave number. Furthermore it is weakly dependent on wave number for $\alpha^* > 6$, equivalent to a boundary-layer thickness δ greater than the pattern wavelength λ, which corresponds to most of the observed crosshatching data. Now from the definition of α^*, τ and κ^* [see Nomenclature and Eq. (14)], the quantity $\alpha^*\tau/\kappa^*$ appearing in the ordinate of Fig. 4 is proportional to $\alpha^{*1/4}/\lambda^{3/4}$ for turbulent flows (since $1/\kappa^* \sim 1/c_f \sim x^{1/5} \sim \delta^{1/4}$) and uniform external boundary-layer conditions. Since for large wave numbers $\alpha^*\tau \cdot \alpha^* c_I^*/\kappa^*$ is insensitive to α^* and $\alpha^*\tau/\kappa^*$ is but a weak function of α^* for a fixed wave length, we conclude that the dimensionless amplification rate $\alpha^* c_I^*$ is also only weakly dependent on $\alpha^* \sim \delta/\lambda$. Therefore the most unstable disturbance wavelength cannot be determined from a condition of maximum amplification rate. The results of Fig. 4 are also typical for higher boundary-layer edge Mach numbers and different wave angles. In addition, for a given wave number the calculated results show that the amplification rate increases monotonically with decreasing wave angle. Therefore, the present theory is unable to predict the preferred wave angle.

An estimate of the behavior of the most unstable wave length may be found from Eq. (13c). The quantity $\alpha^*\tau c_R^*/\kappa^*$ given by this equation is shown in Fig. 5 for the three different Mach number profiles. At the higher wave numbers this term, like the amplification rate term, is only weakly dependent on the wave number. As already pointed out, the wave speed c_R^* has some value less than about 0.5, so that the quantity $\alpha^*\tau/\kappa^*$ may be taken to be essentially independent of α^*. Therefore from the definitions of α^*, τ, and κ^* [see Nomenclature and Eq. (14)]

$$\lambda \sim \mu U_e/p_e M_e^2 c_f \tag{15}$$

i.e., the disturbance wavelength is proportional to the material viscosity, inversely proportional to the surface pressure, and independent of the shear modulus. This result also shows that for turbulent boundary-layer flows with uniform external velocity the pattern wavelength is only weakly dependent on streamwise distance.

In summary, the disturbance flow is unstable for the Maxwell body for the three Mach number profiles considered but the calculation of amplification rates shows that the turbulent profile is most capable of producing a resonant condition, followed in turn by the stepped profile and then by the laminar profile. Resonant conditions are more likely when the edge Mach number normal to the wave is supersonic since the amplification rates are larger than those for subsonic flow. For turbulent boundary-layer flow the pattern wavelength is only weakly dependent on streamwise distance and is proportional to the material viscosity and inversely proportional to the surface pressure. The present inviscid theory is, however, unable to predict the wave speed or the preferred wave angle and a viscous stability analysis may be required to determine these quantities.

III. Data

Prior to the present study only the qualitative nature of crosshatch pattern characteristics was available in the literature. Quantitative pattern measurements, such as thickness and wavelength distributions, had not been made. A new technique was developed to provide detailed surface thickness measurements. The technique involved first making a rubber mold of the crosshatched surface. The second step consisted in making a transparent plastic cast of the surface from the mold. The third step was the recording of the surface pattern geometry on contour plots and magnetic tape by processing the transparent cast through a scanning microdensitometer.§ The magnetic tape data were in turn processed through a number of computer programs. The mean thickness and the standard deviation from the mean were computed for each scan. A program performed a Fourier transform on the data in order to obtain the dominant pattern wavelengths. The program was also capable of plotting the data to obtain two-dimensional plots of thickness vs distance along the scan.

SPARTA Re-Entry Vehicles

Surface patterns were observed on the ablated heat shields of a number of recovered SPARTA conical re-entry vehicles.

§ Carried out by Photometrics Inc., Lexington, Mass.

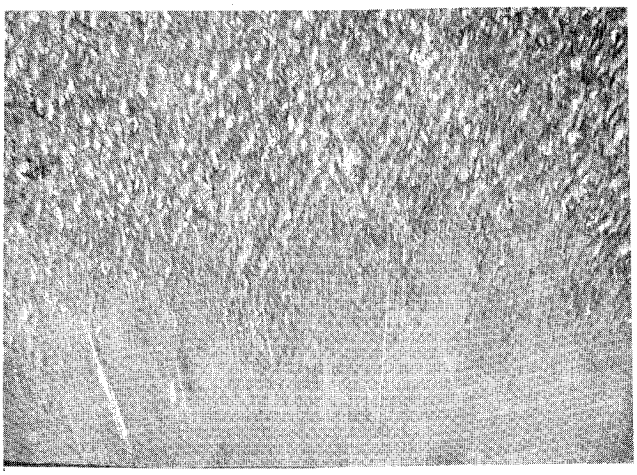

Fig. 6 Crosshatch surface pattern on SPARTA RV-6 recovered re-entry vehicle.

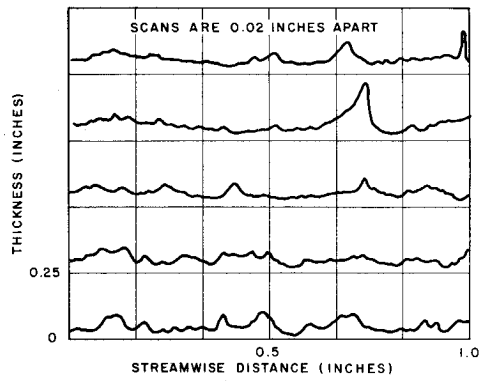

Fig. 7 Typical pattern thickness profiles on SPARTA RV-6 recovered re-entry vehicle.

Details of the postflight analyses together with vehicle and surface pattern data may be found in Ref. 2.

Two silica phenolic vehicles (SPARTA RV-2 and RV-5) exhibited streamwise groove patterns while a Teflon vehicle (SPARTA RV-6) exhibited a crosshatch groove pattern superimposed on a streamwise pattern. In all three cases the streamwise grooves were aligned with the generators of the cones and spaced approximately 5° apart. Fully developed crosshatch patterns appear approximately 8.5 in. from the stagnation point of the RV-6 vehicle (see Fig. 6) and extend to the base of the cone at 34 in. Typical surface thickness profiles towards the rear of the vehicle, as obtained by the technique described previously, are shown in Fig. 7. Although each individual scan indicates a highly irregular behavior, the crosshatch geometry based upon the average pattern statistics does not change appreciably over the length and circumference of the vehicle. The crosshatch half-angle varies between 24 and 26°, the streamwise wavelength as obtained from the Fourier transform of the thickness profile varies between 0.35 and 0.40 in., and the standard deviation pattern thickness is 0.0055 ± 0.00005 in. It is interesting to note that 1 to 2 in. upstream of the fully developed crosshatching, regular diamond shaped patterns of much smaller depth occur having a wave-angle of 29° and a streamwise wavelength of 0.25 in.

Postflight analysis on the RV-6 Teflon vehicle showed that the tip blunted up during re-entry and that the total ablation on that portion of the cone frustum upstream of the crosshatching was very small compared to that on the rest of the body. This indicates that transition never reached the nose and that the boundary layer was probably laminar to the position at which the patterns first appear on the cone surface. This result is consistent with ground test data that crosshatching does not appear when the boundary layer is laminar.

Reference 2 shows that except at very low altitudes the local flow over the RV-6 vehicle is supersonic and that during most of the trajectory the local boundary layer edge Mach number is in excess of 6. The measured pattern angles (24–26°) are considerably larger than the Mach angle of 9.6° corresponding to this Mach number; at the altitude where the ablation terminates the local Mach number is 4 and the Mach angle is 14.5°. That crosshatching appears only when the flow is supersonic is also consistent with ground test data.

Near peak heating the ratio of the boundary-layer thickness at the base of the cone to the pattern wavelength is approximately unity, and the corresponding dimensionless wave number $\bar{\alpha}$ is 6. Since the turbulent boundary-layer thickness grows as $x^{4/5}$ the constant pattern wavelength does not correlate with the boundary-layer thickness. The pattern thickness is of the same order as the laminar sublayer thickness implying that during the later stages of the crosshatching development a nonlinear interaction between the surface and the boundary layer may limit the pattern depth.

Flowfield calculations show that the surface pressure is constant over that portion of the cone where crosshatching appears, even though the tip blunted during re-entry. That the pattern wavelength is constant is consistent with the present inelastic deformation model [see Eq. (15)] as is all of the other data just presented. It is interesting to point out here that in wind-tunnel tests on camphor cones which crosshatched[4] it was found that the pattern wavelength decreased in proportion to the increase in surface pressure, again consistent with the theoretical result of Eq. (15).¶

Roth[2] points out that crosshatching did not develop on the two recovered silica phenolic re-entry vehicles although crosshatch patterns did appear on silica phenolic models tested in the Malta Rocket Exhaust Facility under a less severe pressure and heat transfer environment.[3] He attributes this behavior to disparate melt layer characteristics. A possible alternative explanation follows from the fact that the models tested at Malta had a carbon phenolic tip and a silica phenolic frustum so that a concave rearward facing ramp formed at the juncture of the two materials. The pattern formation was then intimately connected with the longitudinal vortices[21] that developed in the flow due to the surface concavity and not necessarily as a result of the linear inelastic response of the material alone. On the other hand, in the flight case the pressure fluctuations were probably too low to excite the silica phenolic heat shield.

NASA Ames

Nachtsheim and Larson[22] present a systematic investigation of the effect of material properties on crosshatching under the same aerodynamic environment. They tested a number of Teflon and Teflon composite cones in the exhaust jet of a hydrogen-oxygen rocket. The surface Mach number was 3.6 and the surface pressure 22 psia.

The models were made of commercially available forms of Teflon[23] (TFE, FEP, and CTFE) and Teflon TFE filled with varying amounts of borosilicate glass and graphite. The model made of TFE alone exhibited the most pronounced crosshatching. As the percentage of borosilicate glass increased to 25% the depth of the patterns decreased, although the pattern wavelength and angle appeared to remain the same. The pattern geometry was relatively constant on a given model. In all cases there was appreciable ablation.

In another test, with a TFE model containing 25% of a "special fill"[23] the crosshatching was eliminated completely.

¶ Note added in proof: Recently Stock and Ginoux[25] tested cones made of natural wax and camphor in a wind tunnel and found that the pattern wavelengths agree very well with those of Williams,[4] extending the range to larger values of pattern wavelength, or lower static pressure.

This composite is described by the manufacturer as having the "best deformation and tensile properties . . ." and as being used in applications "where the highest antideformation or cold flow properties are required."

Nachtsheim and Larson interpret the test results on the basis of a liquid film stability analysis. An alternative explanation based upon our material response model is possible. The addition of glass increases the resistance of Teflon to deformation and makes the surface more stable to the surface pressure fluctuations even in the presence of appreciable ablation.

For completeness the data obtained by Nachtsheim and Larson which was presented in Ref. 13 is here summarized. The model tested was a Teflon (FEP) cone with the Mach number at the edge of the boundary-layer approximately 2. The boundary layer was turbulent. The material properties were such that for the test conditions the body did not ablate (either sublime or form a discernible liquid melt) but did exhibit creep and relaxation. When the test was begun nothing was seen to happen for the first few seconds, during which time the model heated up. After this period, however, the material softened sufficiently and a crosshatch pattern was observed to break out simultaneously over the entire length of the model. When removed from the tunnel the model showed no mass loss to within the measurement accuracy of 0.1 g for the 650 g cone. The pattern angle was consistent with previous measurements ($\sim 35°$), while the pattern wavelength was around 0.1 in. It is interesting to note that the average recession based upon a maximum weight loss of 0.1 g and the surface area of the cone was approximately 10^{-4} in. which was much smaller than the average depth of the crosshatch patterns. This critical experiment, in which a nonablating inelastic deformable body crosshatched when placed in a supersonic turbulent flow, lends support to the present material response model.

IV. Conclusions

The material response model in which a nonablating, inelastic deformable surface interacts with an external supersonic turbulent boundary layer appears to be capable of predicting many features of observed crosshatch patterns. The model itself has so far only been analyzed for linear relaxing materials and from the point of view of inviscid linear stability theory. This analysis is unable, for example, to give either the disturbance wave speed or the crosshatch pattern angle. Nonetheless it is consistent with available experimental data even if it cannot always predict every feature of the data. The linear stability theory should be extended to a viscous analysis and possibly more complicated materials. A simplified viscous analysis along the lines of Engelund[24] who treated the problem of the instability of erodible beds is suggested. It is expected that the general mechanism of crosshatching is a complicated one containing many nonlinear effects but the deformable relaxing and creeping surface should still form the basis for describing the phenomena.

References

[1] Larson, H. K. and Mateer, G. G., "Cross Hatching—A Coupling of Gas Dynamics with the Ablation Process," AIAA Paper 68-670, Los Angeles, Calif., 1968.

[2] Roth, H., "SPARTA Recovered Vehicle Evaluation Program," Technical Interchange Meeting Report M-280, Feb. 1969, Missile Div., Chrysler Corp., Detroit, Michigan.

[3] Langanelli, A. L. and Nestler, D. E., "Surface Ablation Patterns: A Phenomenology Study," *AIAA Journal*, Vol. 7, No. 7, July 1969, pp. 1319–1325.

[4] Williams, E. P., "Experimental Studies of Ablation Surface Patterns and Resulting Roll Torques," *AIAA Journal*, Vol. 9, No. 7, July 1971, pp. 1315–1321.

[5] Canning, T. N., Wilkins, M. E., and Tauber, M. E., "Ablation Patterns on Cones Having Laminar and Turbulent Flows," *AIAA Journal*, Vol. 6, No. 1, Jan. 1968, pp. 174–175.

[6] Donaldson, C. duP., "Boundary Layer Resonance Analysis," *RVTO Roll Phenomenology*, Sect. 8, Re-entry Systems Div. Doc. 68DS809, 1968, General Electric Co., Valley Forge, Pa.

[7] Conrad, P. W., Donaldson, C., and Snedeker, R., "A Study of the Modal Response Approach to Patterned Ablation Including Experiment Definition," SAMSO-TR-70-213, April 1970, Aeronautical Research Associates of Princeton, Princeton, N. J.

[8] George, D., *Inviscid Stability of Supersonic Boundary Layers with Ablative Surface Coupling*, M.S. thesis, 1969, Illinois Inst. of Technology, Chicago, Ill.

[9] Inger, G. R., "Discontinuous Supersonic Flow Past an Ablating Wavy Wall," *AIAA Journal*, Vol. 7, No. 4, April 1969, pp. 762–764.

[10] Lees, L. and Kubota, T., "Research on Fluid Mechanics of Striating Ablation," GALCIT Progress Rept. Nos. 1, 2, and 3, 1969, California Inst. of Technology, Pasadena, Calif.

[11] Lew, H. G. and Li, H., "The Role of the Turbulent Viscous Sublayer in the Formation of Surface Patterns," Missile and Space Div. Rept. R68SD12, Aug. 1968, General Electric Co., Valley Forge, Pa.

[12] Nachtsheim, P. R., "Analysis of the Stability of a Thin Liquid Film Adjacent to a High-Speed Gas Stream," TN D-4976, Jan. 1969, NASA.

[13] Probstein, R. F. and Gold, H., "Cross-Hatching: A Material Response Phenomena," *AIAA Journal*, Vol. 8, No. 2, Feb. 1970, pp. 364–366.

[14] Lin, C. C., *The Theory of Hydrodynamic Stability*, Cambridge University Press, Cambridge, 1955, pp. 1–14, 67–82.

[15] Squire, H. B., "On the Stability of Three-Dimensional Disturbances of Viscous Flow Between Parallel Walls," *Proceedings of the Royal Society of London, Ser. A*, Vol. 142, No. A847, Nov. 1963, pp. 621–628.

[16] Dunn, J. J. and Lin, C. C., "The Stability of the Laminar Boundary Layer Equations in a Compressible Fluid for the Case of Three-Dimensional Disturbances," *Journal of the Aeronautical Sciences*, Vol. 19, No. 7, July 1952, p. 491.

[17] Benjamin, T. B., "Shearing Flow Over a Wavy Boundary," *Journal of Fluid Mechanics*, Vol. 6, Pt. 2, Aug. 1959, pp. 161–205.

[18] Freudenthal, A. M., *The Inelastic Behavior of Engineering Materials and Structures*, Wiley, New York, 1950, pp. 220–231.

[19] Lees, L. and Reshotko, E., "Stability of the Compressible Laminar Boundary Layer," *Journal of Fluid Mechanics*, Vol. 12, Pt. 4, April 1962, pp. 555–590.

[20] Lees, L. and Gold, H., "Stability of Laminar Boundary Layers and Wakes at Hypersonic Speeds," *Proceedings of the International Symposium on Fundamental Phenomena in Hypersonic Flow*, edited by J. Gordon Hall, Cornell University Press, Buffalo, N. Y., 1966, pp. 310–342.

[21] Tobak, M., "Hypothesis for the Origin of Cross Hatching," *AIAA Journal*, Vol. 8, No. 2, Feb. 1970, pp. 330–334.

[22] Nachtsheim, P. and Larson, H. K., "Crosshatched Ablation Patterns in Teflon," *AIAA Journal*, Vol. 9, No. 8, Aug. 1971, pp. 1608–1614.

[23] *Teflon*, Saunders, Los Angeles, Calif., 1968.

[24] Engelund, F., "Instability of Erodible Beds," *Journal of Fluid Mechanics*, Vol. 42, Pt. 2, June 1970, pp. 225–244.

[25] Stock, H. W. and Ginoux, J. J., "Experimental Results on Crosshatched Ablation Patterns," *AIAA Journal*, Vol. 9, No. 5. May 1971, pp, 971–972.